Available online at www.sciencedirect.com
ScienceDirect
Journal of Power Sources 161 (2006) 730–736
JOURNAL OF POWER SOURCES
www.elsevier.com/locate/jpowsour

Nanostructured mesoporous carbon as electrodes for supercapacitors

S.R.S. Prabaharan [a,*], R. Vimala [b], Zulkarnian Zainal [c]

[a] *School of Electrical and Electronics Engineering, Faculty of Engineering and Computer Science, The University of Nottingham Malaysia Campus, Jalan Broga, 43500 Semenyih, Selangor, Malaysia*

[b] *Material Characterization Department, S.E.H. Malaysia Sdn. Bhd Lot 2, Lorong Enggang 35, Ulu Klang Free Trade Zone, 54200 Selangor, Malaysia*

[c] *Department of Chemistry, Faculty of Science, Universiti Putra Malaysia, Serdang, Malaysia*

Received 3 November 2005; received in revised form 27 March 2006; accepted 28 March 2006
Available online 5 June 2006

Abstract

Symmetrical carbon/carbon double layer capacitors (EDLCs) were fabricated employing nanostructured mesoporous nongraphitized carbon black (NMCB) powders and their EDLC behavior was studied using electrochemical techniques viz., cyclic voltammetry, a.c.-impedance, and constant current cycling. Rectangular shape cyclic characteristics were observed indicating the double layer behavior of the NMCB carbon electrodes. The mechanism of double layer formation and frequency dependent capacitance were deduced from the ac-impedance analysis. Specific capacitance, power density and energy density were derived from constant current charge/discharge measurements. NMCB powders demonstrated a specific capacitance of about $\sim$39 F g^{-1} and the power density of 782 W kg^{-1} at a current density of 32 mA cm^{-2}. Nevertheless, at a low current density (3 mA cm^{-2}), the specific capacitance of $\sim$44 F g^{-1} was achieved, which corroborates with the values obtained by means of ac-impedance (40 F g^{-1}) and cyclic voltammetry (41.5 F g^{-1}). The test cells demonstrated the stable cycle performance over several hundreds of cycles.

Keywords: Mesoporous carbon; Carbon electrodes; Supercapacitors; Nanostructure; Electrochemical properties

1. Introduction

Supercapacitors (SCs) or electrochemical capacitors (ECs) based on double-layer capacitance store energy in a polarized double layer with a separation of only a few angstroms thick at the interface between an ionically conducting electrolyte solution and an electronically conducting electrode. The separation of charge in the ionic species at the interface (called an electric double layer) produces a standing electric field establishing an electric double layer capacitance, EDLC. The crucial factor behind the high capacitance in EDCLs is the presence of a large electrode area. Carbonaceous materials have attracted increased interest as promising electrode material for supercapacitors due to their high surface area, highly porous nature, in addition to long cycle life and high power density [1–5]. There are various types of carbonaceous compounds used as electrodes for SCs (e.g., activated carbon, carbon black (CB), carbon fiber cloth, graphite powder, glassy carbon and carbon aerogel). They were used as sole electrode component in supercapacitor or as part of composite electrodes that contain pseudocapacitance materials such as RuO_2 [6,7]. Carbons for supercapacitors must have high specific areas, good intra- and interparticle conductivity in porous matrices, good electrolyte accessibility to intrapore surface area, good bulk electrical conductivity and minimum self-discharge rate [8]. Recently, Chu and Braatz considered many of the current supercapacitor systems [9].

Recently, a great interest has been focused on the application of nanostructured carbons for the energy storage applications. The use of nanostructured nongraphitized carbons has the advantage of providing a large specific surface area due to their mesoporosity. Of late, the nanostructured materials are gaining popularity in energy storage devices, particularly in electrochemical capacitors. The application of different types of nanostructured carbons for fabricating EDLCs proves the high ability of this material for charge accumulation at the electrode/electrolyte interface, the so-called "double-layer".

Frackowiak et al. [10] reported that the supercapacitor electrodes prepared from single-walled carbon nanotubes (SWNTs) achieved a value of 40 F g^{-1}, i.e. twice smaller than for multi-

* Corresponding author. Tel.: +603 8924 8125; fax: +603 8924 8017.
E-mail address: prabaharan.sahaya@nottingham.edu.my (S.R.S. Prabaharan).

0378-7753/$ – see front matter © 2006 Elsevier B.V. All rights reserved.
doi:10.1016/j.jpowsour.2006.03.074

walled carbon nanotubes (MWNTs) which offered a capacitance of 80 F g^{-1}. Park et al. [11] have synthesized carbon nanotubes by plasma enhanced chemical vapor deposition (PECVD) as EC electrode material. They obtained a specific capacitance in the range of 33–82 F g^{-1} using non-aqueous aprotic organic solvent, $LiPF_6$/EC/DEC. While, Diederich et al. [12] reported another form of nanostructured material, a carbon film grown at room temperature by supersonic cluster beam which showed a specific capacitance of 75 F g^{-1}. All these involved an expensive proposition to produce the nanostructured carbons. Although the above approach appears to be promising in order to obtain high capacitance values in the form of EDLCs, the cost factor in producing these nanocarbons (especially single-walled and multiwalled carbon nanotubes) is indeed high as yet.

On the other hand, porous carbons have been extensively investigated as electrodes for supercapacitors because of their low cost and potential for high-energy storage densities. The major attraction of porous carbon electrodes is that they can be prepared with very high surface areas. However, since high surface area porous carbons typically have a high fraction of micropores (pore size, <2 nm), only a part of the surface of the carbon is effectively utilized; most of the surface therefore does not contribute to the double-layer capacitance of the electrode and the measured capacitance values are therefore only about 20% of theoretical. To effectively address this issue, there were efforts to develop mesoporous carbons for ultracapacitors or supercapacitors [13–15]. Accordingly, the present work is centered on investigating nongraphitized NMCBs as electrodes for the electrochemical capacitors (EC).

We report here our success in identifying a new mesoporous carbon having modest BET surface area (469 m^2 g^{-1}), which could be regarded as a candidate electrode for EDLC applications. As part of our systematic approach, we have characterized the MCB by means of physical (XRD, BET), microstructural (SEM, TEM) techniques. The electrical conductivity was also measured using conventional four-probe technique. The specific capacitance, energy and power densities were measured by fabricating the symmetric electrode electrochemical capacitors employing an aqueous electrolyte. The rationale for choice of aqueous electrolyte media is that the carbon materials with a narrow pore size distribution at about 10 nm and the particle size in the nanometric range are specially adapted for EDLC—electrodes in aqueous media, as they combine large amounts of energy with high power density.

2. Experimental details

2.1. Electrode preparations

The NMCB namely Monarch 1400 carbon black was kindly supplied by Cabot Inc., (Malaysia) and used as received to fabricate carbon electrodes. The BET specific surface area, micropore volume, average pore size, average particle sizes, bulk density and conductivity of Monarch 1400 were investigated. Electrodes were composed of 90 wt.% carbon black and 10 wt.% of polyvinylidene fluoride (PVdF) (Elf Atochem, France). The Monarch 1400 powders were added to PVdF/acetone mixture and the mixture was stirred to form a carbon slurry. NMCB electrodes were fabricated by coating the slurry on the copper mesh (Exmet, USA) that acts as the current collector. Then, 3.14 cm^2 circular discs were punched out from the coating and dried overnight in the vacuum oven.

2.2. Cell constructions

Sandwich-type symmetric capacitor cells were constructed with a pair of electrodes and a piece of filter paper (Whatman® grade 1) as separator. As for the electrolyte, 2 M NaOH aqueous solution was prepared and used as electrolyte. Prior to cell construction, electrode pellets were vacuum wetted (degassed) in the electrolyte solution (aqueous 2 M NaOH) for an hour. The degassing of the electrodes was carried out in order for the electrolyte to reach the distributed mesopores effectively so as to enhance the dense ionic double layer across the interface.

2.3. Electrochemical measurement

The electrochemical impedance spectroscopy (EIS) measurements were carried out using Basic Electrochemical System (BES), Perkin-Elmer, USA An ac perturbation amplitude of 10 mV was used and the data were collected in the frequency range of 10 mHz–10 kHz. The electrochemical performance of the symmetrical capacitors was evaluated by means of cyclic voltammetry and constant current charge/discharge by employing Arbin Battery Testing System (BT2000, USA). All the electrochemical measurements were conducted at room temperature.

3. Results and discussion

3.1. Powder XRD and HR-TEM

X-ray diffraction (XRD) patterns (10°–60°) were obtained using JEOL (model JDX 8030) X-ray diffractometer equipped with a diffracted beam monochromater (Cu Kα radiation, $\lambda = 1.5418$ Å). Fig. 1 displays the wide-angle XRD patterns of NMCB powder. The NMCB shows broad diffraction peaks exhibiting the typical disordered structure, with characteristic peaks at $2\theta = 24°$ and 44° that are related to the (0 0 2) and (1 0 0)

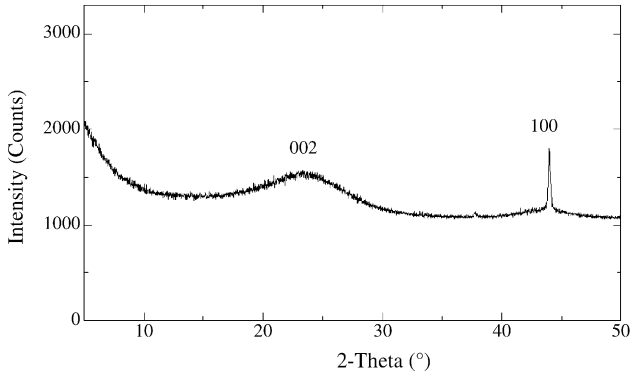

Fig. 1. XRD patterns of Monarch 1400 mesoporous carbon black powders.

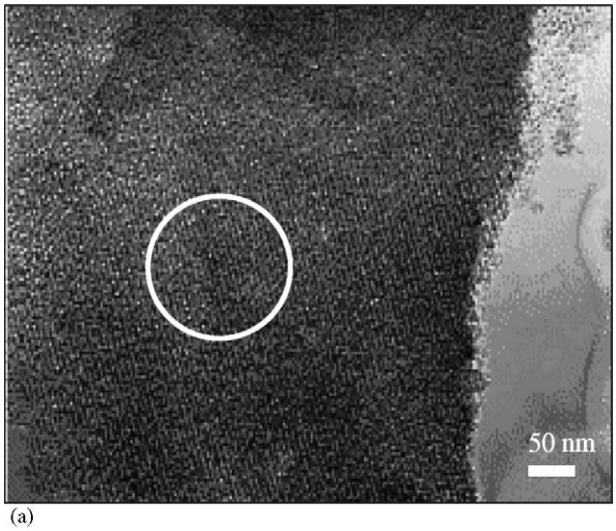

Fig. 2. (a) HRTEM image showing the lattice image exhibiting the fringe pattern obtained on MONARCH 1400 mesoporous carbon black. The disordered fringes are seen clearly as indicated in the circle confirming the amorphous nature. (b) HRTEM picture of Monarch 1400 having mesopore structure with honeycomb pattern.

reflections, respectively. The location and broadness of the peaks suggested a disorder structure of the NMCB.

The nanostructure of carbon black was examined by means of a JEOL 1200EX transmission electron microscope (TEM). The HRTEM image as depicted in Fig. 2a shows the lattice image exhibiting the fringe pattern that explicitly reveals the disordered lattice planes (*d* spacing) together with disordered nanostructure indicating the amorphous nature. The nanostructure morphology of Monarch 1400 is shown in Fig. 2b. The distribution of narrow pores is evident from the magnified image (Fig. 2b), which exhibits honeycomb morphology with physical pore diameter ranges between 10 and 15 nm as shown in Fig. 2b.

The specific surface area, micropore volume and average pore size of Monarch 1400 were calculated from nitrogen, N_2 adsorption–desorption isotherms ((Micrometrics ASAP 2010) using the Brunauer-Emmet-Teller (BET) procedure The BET surface area determined for Monarch 1400 is 469 $m^2\,g^{-1}$. The BET specific surface area, micropore volume, average pore size, average particle sizes, bulk density and conductivity of Monarch 1400 are summarized in Table 1.

Table 1
Physical properties of Monarch 1400 carbon

Trade name of carbon	Monarch 1400
BET Surface area ($m^2\,g^{-1}$)	469.215
Micropore area ($m^2\,g^{-1}$)	145.748
Micropore volume ($cc\,g^{-1}$)	0.066
Average pore size (Å)	66.368
Particle size (nm)	13
Bulk density ($kg\,m^{-3}$)	336.39
Conductivity ($S\,cm^{-1}$)	19.70

3.2. Electrochemical impedance spectroscopy (EIS)

The electrochemical impedance spectrum was measured in the frequency range 10 kHz–10 mHz. The Nyquist complex plane impedance plot, Z″ (real) versus Z′ (imaginary) is presented in Fig. 3. The complex plane plot consists of a small semicircle at high frequencies (bulk *RC* response) followed by a vertical spike at low frequency region indicating the pure double layer capacitive (C_{dl}) behavior. However, there is a discontinuity between the bulk response (semicircle) and the double layer low frequency spike as shown in Fig. 3 as will be explained later. Due to steep vertical sloping of the double layer spike, the Warburg tail which is expected to occur with 45° inclination is not seen clearly although the Warburg response arises as a result of the distributed resistance in the porous electrode structure. As for the double layer spike, the non-ideality of this vertical slope is due to the surface roughness and non-uniform active layer thickness.

As for impedance plot, the high frequency arc is the overall contact impedance generated from the electrical connection between active particles and the current collector as well as change in electrolyte resistance within pores. Further, it has been observed that there is a discontinuity between the semicircle (charge transfer) portion and the vertical line (double layer regime). The origin of this discontinuity, although not

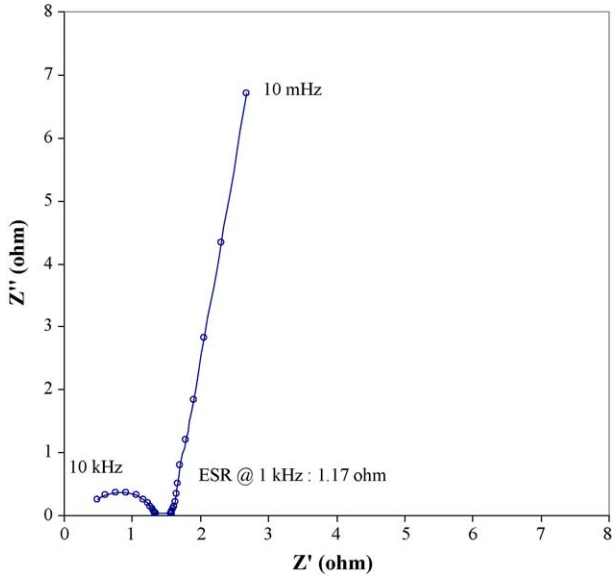

Fig. 3. Nyquist complex impedance plots (Z′ (real) vs. Z″(imaginary)).

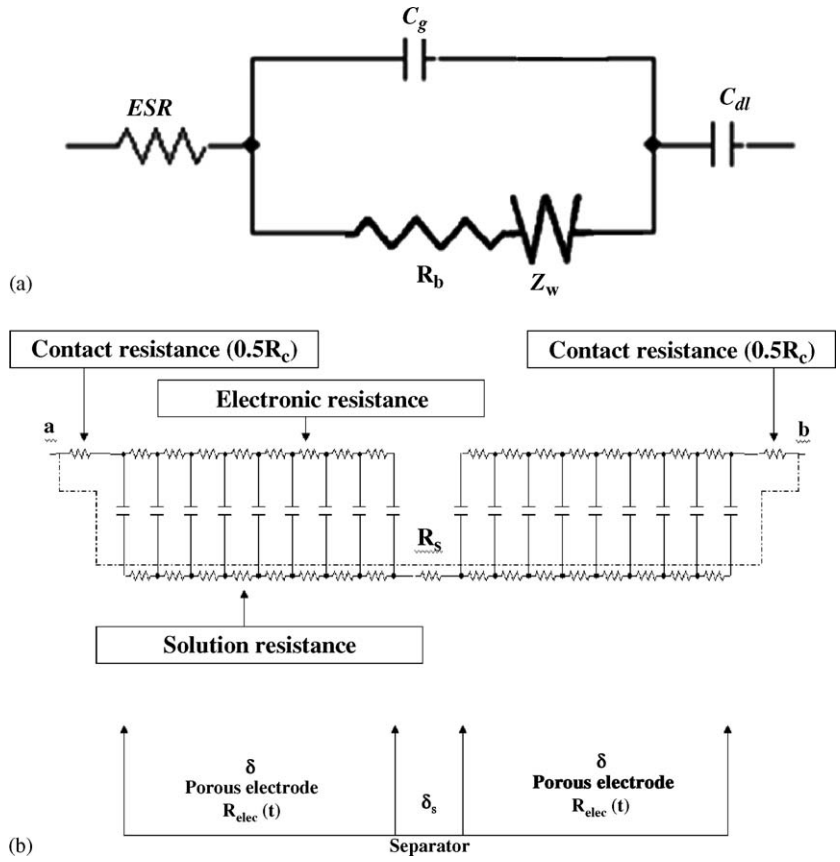

Fig. 4. Simplified equivalent circuit describing the various electrical elements involved in porous EDLCs. (a) A simple circuit model illustrating the presence of various resistive and capacitive elements present in an EDLC employing highly porous symmetric electrodes.

clear, probably caused by the diffusion limited propagation time delay of the signal reaching the double layer via the electrode/electrolyte interface into long mesopores. The double layer capacitive behavior (vertical line) starts at about ~8 Hz down to the lowest frequency value studied (10 mHz).

The impedance plot may be represented adequately according to a geometric capacitance (C_g) with a bulk resistance (R_b), equivalent series resistance (ESR), Z_W represents the finite length Warburg impedance due to distributed resistance within the mesopores and a double layer capacitance (C_{dl}) which are illustrated in the simplified equivalent circuit as shown in Fig. 4. The ESR value was measured at 1 kHz. In porous electrodes, the ESR in general is a summation of $R_{contact} + R_{electrolyte} + R_{bulk\ electrode} + R_{pore} + R_{separator}$. A simple circuit model illustrating the presence of various resistive and capacitive elements present in an EDLC employing highly porous symmetric electrodes is shown in Fig. 4a. This circuit model represents a continuous distribution of capacitance and resistance through the highly porous electrodes. A similar model has recently been proposed by Mark W. Verbrugge et al. [16].

In the present study, we have estimated the value of ESR at 1 kHz for Monarch 1400 is 1.17 mΩ. Due to intrinsic porous nature of MCB, the propagation of the signal into inner pore structures includes longer electrolyte pathways, which consequently affect the ESR. The frequency dependant capacitance (C_{freq}) was derived from Eq. (1) where ω denotes the angular frequency of the applied ac signal. The value of frequency dependant specific capacitance calculated for Monarch 1400 is 40 F g^{-1}.

$$|C = 1/\omega Z''| \quad (1)$$

In Fig. 5, *RC* plot of capacitance versus resistance is presented. *RC* plot in general renders detailed information on the charging characteristics of the electrode. According to theoretical treatise on impedance response of porous electrode, the ac signal is increasingly propagating into inner pore sites of the electrodes, with decreasing frequency. The NMCB electrodes possessed two interpenetrating phases and the two distinct slopes in region I and II could be attributed to the propagation of signal into two regions with different pore dimensions. In region I, the propagation occurs along the more expanded mesopore structures and the region II can be ascribed to the penetration of ac signal into the narrow mesopores. The *RC* plots reveal the optimized charging characteristics of the NMCB electrodes.

3.3. Cyclic voltammetry

Cyclic voltammograms (CV) obtained between 0.2 and 1 V potential range at different scan rates are shown in Fig. 6. Achieving rectangular-shaped cyclic voltmmograms over a wide range of scan rates is the ultimate goal in EDLC. This behaviour is

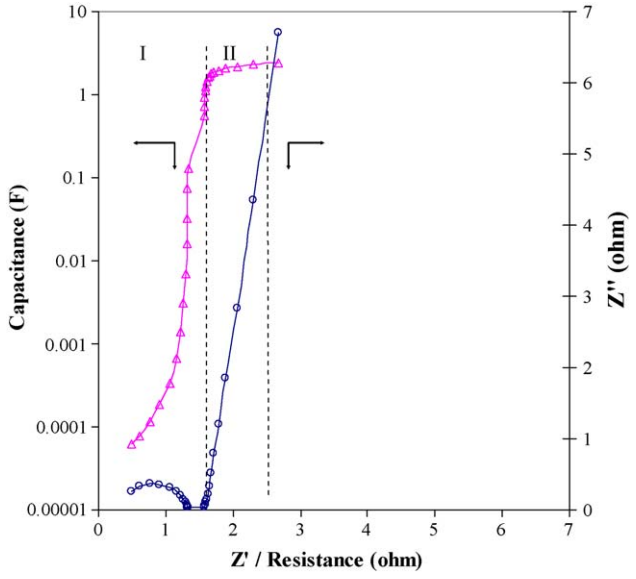

Fig. 5. *RC* plot of capacitance vs. impedance response.

important for practical applications involving high energy and power density. Interestingly, the CV curves show the typical capacitor-like characteristics in the form of almost rectangular cyclic behavior. These results indicate that the charge-discharge responses of the electric double layer are highly reversible. However, in the present case, the CV did not keep the rectangular-shape at a scan rate say, 50 mV s^{-1}. This behavior is clearly attributed to the time constant. That is, if $\tau \neq 0$, the current contains a transient part, which falls exponentially with *RC* time constant where $R = \text{ESR}$, and a steady-state current (*sC*, where *s* is the scan rate and *C* is the double layer capacitance) [17,18]. Also, as τ becomes larger, the transient part lasts longer meaning that more time is required to charge the capacitor), resulting in the collapse of the rectangular shape of the current profiles.

It is commonly accepted that at carbon double layer capacitor electrodes the faradaic (pseudocapacitance) component is of the order 10–20% of the total capacitance. By definition, a pseudocapacitative process is a faradaic process that results in a capacitative response despite involving electron transfer. However, we have not observed any pseudocapacitance contribution in the present studies. There was no pseudocapacitance

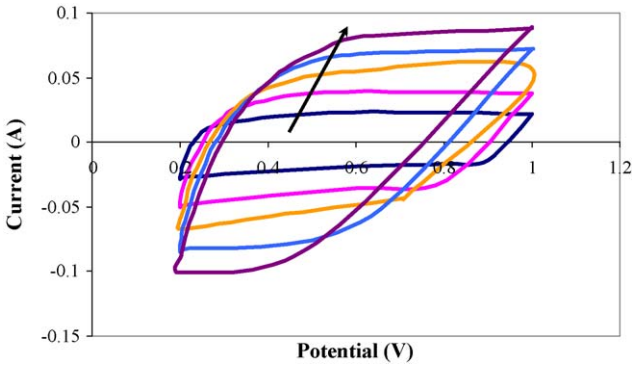

Fig. 6. Cyclic voltammograms of Monarch 1400 at various scan rates (10, 20, 30, 40 and 50 mV s^{-1}). Arrow indicates increasing scan rates.

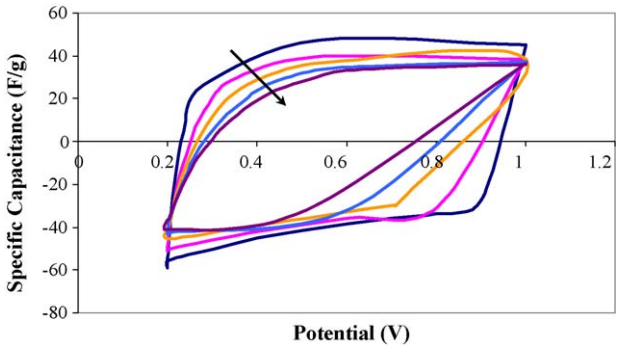

Fig. 7. Specific capacitance vs. cell potential at various scan rates (10, 20, 30, 40 and 50 mV s^{-1}) Arrow indicates increasing scan rates.

observed at a constant rate over a complete cycle, which indicates the capacitance measured is purely capacitive. In this type of energy storage, the phenomenon is purely electrostatic and current is independent of the potential.

On the other hand, as for the CV profiles, the current rising and decaying from the plateau values become gradually depressed with increasing scan rate (see Fig. 6). The above behavior shows less reversible character of this electrode due to the fact that the voltage signal could not reach the pores effectively under increased scan rate, *s*. Consequenctly, the capacitance decreases with sweep rate is because of the high *iR*. This phenomenon is expected to occur due to the distributed capacitance effect in the nanoporous electrodes. The depression of current profiles caused by increased scan rates, *s* may have caused by the difference between the ohmic resistance of the electrolyte at the top of mesopores and at the bottom of mesopores. That is, if any capacitor system has a large *RC* time constant, the rate capability is poor. This feature is ascertained by the CV profiles as shown in Fig. 6, whereby the exponential transient appearing before the plateau becomes longer because more time is required to charge the capacitor [19]. Note that the charge–discharge current of the electric double layer is directly proportional to the scan rate. Obviously, the *iR* drop due to the electrolyte resistance within these mesopores is expected to become significant at a higher scan rate of CV.

Fig. 7 (specific capacitance versus potential) shows scan rate dependence of specific capacitance for Monarch 1400 electrode. The specific capacitance of this Monarch 1400 electrode measured at a scan rate of 20 mV s^{-1} is equal to 41.52 F g^{-1}. Note that an obvious degradation in specific capacitance of Monarch 1400 electrode with increasing scan rate is clearly observed. This is reasonably attributed to the mesoporous nature of Monarch 1400 since the rate of ion rearrangements in the electric double layer is not as fast as the rate of the potential change (i.e. CV scan rate), high *iR* drop caused by ESR and the low capacitance value is associated with *iR* drop and also with the distributed resistance down the pore.

3.4. Galvanostatic charge/discharge cycle

The composite electrode made of Monarch 1400 was subjected to the galvanostatic charge–discharge test to evaluate

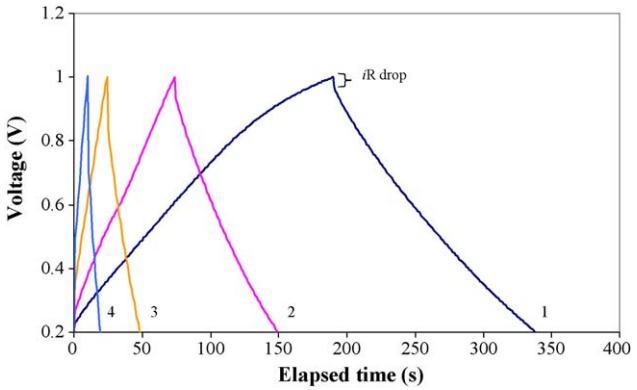

Fig. 8. Galvanostatic charge/discharge cycles at different current densities. (1) 3 mA cm^{-2}, (2) 6 mA cm^{-2}, (3) 16 mA cm^{-2} and (4) 32 mA cm^{-2}.

Table 2
Specific capacitance of Monarch 1400 at different discharge current densities

Current densities (mA cm^{-2})	Specific capacitance (F g^{-1})
3	44.3
6	43.9
16	41.2
32	39.3

Table 3
Summary of specific capacitance value for Monarch 1400 electrodes deduced from different electrochemical techniques

Electrochemical technique	Specific capacitance (F g^{-1})
AC impedance	40.0
Cyclic voltammetry	41.5
Galvanostatic discharge at 3 mA cm^{-2}	44.3
Galvanostatic discharge at 32 mA cm^{-2}	39.3

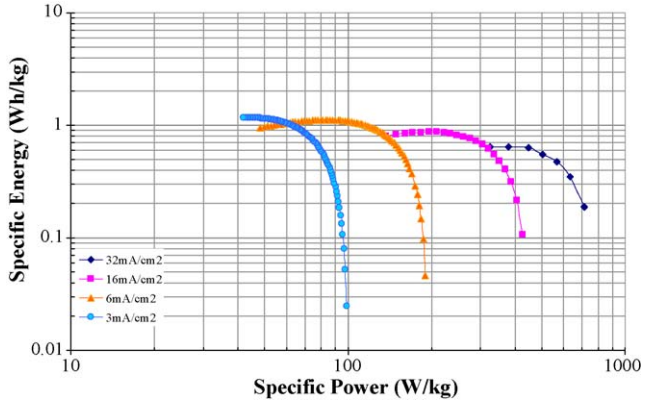

Fig. 9. Ragone plot attained at various current densities (3–32 mA cm^{-2}).

its capacitive behavior and the results obtained at various current rates are displayed in Fig. 8. At low discharge current, the response of the capacitor approaches the ideal linear charge–voltage relationship. At higher current rate, the total impedance of the cell gives rise to initial drop of the discharge voltage, which remains until the constant capacitive performance is reached. The low capacity values observed at higher current rates are associated with *iR* drop within the capacitors. The *iR* drop as indicated in the Fig. 8 is a direct measure of ESR which influences the overall power performance of a capacitor cell.

Specific capacitance of the electrode was obtained from $C = (I \times t)/(W \times \Delta E)$ where I is the discharge current, t is the discharge time, W is the mass of active material on one electrode, and ΔE is the potential difference during discharge excluding the portion of *iR* drop. The measured specific capacitances of Monarch 1400 electrode at different discharge current densities are summarized in Table 2. Table 3 summarizes the specific capacitance values achieved for Monarch 1400 employing different electrochemical techniques.

Nomoto et al. [20], summarizes representative relationships of specific surface area (m^2 g^{-1}) of carbon to specific capacitance (F g^{-1}) in a plot. From the plot, the activated carbon with approximate surface area of 600 m^2 g^{-1} has as an approximate value of 10 F g^{-1} as specific capacitance. In comparison, Monarch 1400 MCB (469.22 m^2 g^{-1}) showed much higher capacitance of about 40 F g^{-1} (four times greater). To confirm the cycling stability of the Monarch 1400 electrodes, supercapacitors were cycled at 6 mA cm^{-2} in the range between 0.2 and 1.0 V.

3.5. Ragone plot

Ragone plot represents the dependence of achieved specific energy density versus specific power density, the latter being determined by the rates at which discharging of an electrical energy storage device are conducted in general and the EDLC devices in particular. Fig. 9 shows the Ragone plot for Monarch 1400 symmetrical capacitor attained from the constant current discharge at specific current rates. Specific energy density and specific power density values were calculated by taking into account of the total composite masses, according to the equations, $E(\text{Wh kg}^{-1}) = [i(\text{A}) \times V(\text{V}) \times t(\text{h})]/\text{m(kg)}$ and $P(\text{W kg}^{-1}) = [i(\text{A}) \times V(\text{V})]/\text{m(kg)}$, respectively where i is discharge current, V is voltage excluding the *iR* drop occurring at the beginning of the discharge (Fig. 8), t is time in hour and m is the mass.

The obtained power density and energy density values at typical discharge current rates (3 and 32 mA cm^{-2}) are summarized in Table 4. The constant discharge at 32 mA cm^{-2} yielded a power density of 782.42 W kg^{-1} which is reasonably a high

Table 4
Specific capacitance, energy and power density at 3 and 32 mA cm^{-2}

Discharge current densities (mA cm^{-2})	Specific capacitance (F g^{-1})	Specific energy (Wh kg^{-1})	Specific power (W kg^{-1})
3	44.29	1.16	98.84
32	39.30	0.64	782.42

value. Obviously, the higher power density is achievable with higher current rates. However, the energy density is very low at high current density, which is much expected for supercapacitors employing aqueous electrolytes, which limit the operating voltage to 1.0 V. Such supercapacitors are typically suitable for pulse power applications, which involve high rate discharges.

4. Conclusions

The electrochemical properties of NMCB electrodes were investigated by means of impedance spectroscopy, cyclic voltammetry and galvanostatic charge/discharge techniques. Interestingly, the measured specific capacitance values obtained using the above methods are very much comparable. That is, the frequency dependent capacitance deduced from the impedance spectra is 40 F g^{-1}, a value of 41.5 F g^{-1} (scan rate: 20 mV s^{-1}) was obtained from CV and the constant current charge/discharge technique yielded a values of 41.2 F g^{-1} at 16 mA cm^{-2}. The results suggest that the present mesoporous carbon could be useful as candidate for the development EDLCs despite their modest surface area.

Acknowledgements

The authors thank Paul Lim of Cabot (Malaysia) for donating MCBs and for his helpful discussions about the carbons supplied. One of us (VR) thanks Motorola foundation (Malaysia) for assistantship to carry out M.EngSc research degree.

References

[1] R. Kotz, M. Carlen, Electrochim. Acta. 45 (2000) 2483.
[2] W. Sugimoto, T. Shibutani, Y. Murakami, Y. Takasu, Electrochem. Solid-State Lett. 5 (2002) A170.
[3] H. Yang, M. Yoshio, K. Isono, R. Kuramoto, Electrochem. Solid-State Lett. 5 (6) (2002) A141–A144.
[4] A. Nishino, J. Power Sources 60 (1996) 137.
[5] M. Endo, Y.J. Kim, K. Osawa, K. Ishii, T. Inoue, T. Nomura, N. Miyashita, M.S. Dresselhaus, Electrochem. Solid-State Lett. 6 (2) (2003) A23–A26.
[6] N.L. Wu, S.Y. Wang, J. Power Sources 110 (2002) 233–236.
[7] F. Cao, J. Prakash, J. Power Sources 92 (2001) 40–44.
[8] B.E. Conway, Electrochemical Supercapacitors, Kluwer-Plenum Publishing Co, New York, 1999.
[9] A. Chu, P. Braatz, J. Power Sources 112 (2002) 236.
[10] E. Frackowiak, K. Jurewicz, S. Delpeux, F. Beguin, J. Power Sources 97 (2001) 822–825.
[11] D. Park, H.K. Young, K.L. Joung, Carbon 41 (2003) 1025–1029.
[12] L. Diederich, E. Barborini, P. Piseri, J. Appl. Phys. Lett. 75 (1999) 2662.
[13] S. Yoon, J. Lee, T. Hyeon, S.M. Oh, J. Electrochem. Soc. 147 (2000) 2507.
[14] S. Shiraishi, H. Kurihara, A. Oya, Carbon Sci. 1 (2001) 133.
[15] H. Zhou, S. Zhu, M. Hibino, I. Honma, J. Power Sources 122 (2003) 219.
[16] M.W. Verbrugge, P. Liu, S. Soukiazian, J. Power Sources 141 (2005) 369.
[17] L.G. Austin, E.G. Gagnon, J. Electrochem. Soc. 120 (1973) 251.
[18] E.G. Gagnon, J. Electrochem. Soc. 120 (1973) 1052.
[19] A.J. Bard, L.R. Faulkner, Electrochemical Methods: Fundamentals and Applications, Wiley, New York, USA, 1980, pp. 11–15.
[20] S. Nomoto, H. Nakata, K. Yoshioka, A. Yoshida, H. Yoneda, J. Power Sources 97 (2001) 807.